Original Article

MOLECULAR METABOLISM

Low aerobic capacity in McArdle disease: A role for mitochondrial network impairment?

M. Villarreal-Salazar [1,2,11], A. Santalla [3,11], A. Real-Martínez [1,2], G. Nogales-Gadea [4], P.L. Valenzuela [5], C. Fiuza-Luces [5], A.L. Andreu [6], J.C. Rodríguez-Aguilera [3,10], M.A. Martín [2,7], J. Arenas [7], J. Vissing [8], A. Lucia [9], T.O. Krag [8,**], T. Pinós [1,2,*]

ABSTRACT

Background: McArdle disease is caused by myophosphorylase deficiency and results in complete inability for muscle glycogen breakdown. A hallmark of this condition is muscle oxidation impairment (e.g., low peak oxygen uptake (VO_{2peak})), a phenomenon traditionally attributed to reduced glycolytic flux and Krebs cycle anaplerosis. Here we hypothesized an additional role for muscle mitochondrial network alterations associated with massive intracellular glycogen accumulation.

Methods: We analyzed in depth mitochondrial characteristics-content, biogenesis, ultrastructure-and network integrity in skeletal-muscle from McArdle/control mice and two patients. We also determined VO_{2peak} in patients (both sexes, N = 145) and healthy controls (N = 133).

Results: Besides corroborating very poor VO_{2peak} values in patients and impairment in muscle glycolytic flux, we found that, in McArdle muscle: (a) damaged fibers are likely those with a higher mitochondrial and glycogen content, which show major disruption of the three main cytoskeleton components-actin microfilaments, microtubules and intermediate filaments-thereby contributing to mitochondrial network disruption in skeletal muscle fibers; (b) there was an altered subcellular localization of mitochondrial fission/fusion proteins and of the sarcoplasmic reticulum protein calsequestrin-with subsequent alteration in mitochondrial dynamics/function; impairment in mitochondrial content/biogenesis; and (c) several OXPHOS-related complex proteins/activities were also affected.

Conclusions: In McArdle disease, severe muscle oxidative capacity impairment could also be explained by a disruption of the mitochondrial network, at least in those fibers with a higher capacity for glycogen accumulation. Our findings might pave the way for future research addressing the potential involvement of mitochondrial network alterations in the pathophysiology of other glycogenoses.

Keywords McArdle disease; Skeletal muscle; Glycogen; Aerobic capacity; Cytoskeleton and mitochondrial network

1. BACKGROUND

McArdle disease, also known as glycogen storage disease (GSD) type V (OMIM® database number 232600, ORPHA:368) or 'myophosphorylase deficiency' is an autosomal recessive disorder caused by pathogenic mutations in the gene (*PYGM*) encoding the skeletal muscle isoform of glycogen phosphorylase (EC 2.4.1.1), commonly known as 'myophosphorylase'. This condition is one of the most prevalent GSDs, affecting 1:50,000 to 1:200,000 people [1,2]. Because myophosphorylase catalyzes the rate-limiting step in muscle glycogen metabolism by releasing glucose-1-phosphate from the terminal alpha-1,4-glycosidic bond, patients' muscle fibers are unable to obtain energy from intracellular glycogen stores, with subsequent impairment in glycolytic flux. Of note, however, the latter is not fully impeded since fibers can metabolize blood-borne glucose because the metabolic block occurs upstream of blood glucose uptake.

A hallmark of McArdle disease is impairment of muscle aerobic metabolism, as reflected by very low levels of peak oxygen uptake (VO_{2peak}) in most patients, usually below 50% of age and gender-predicted values [3,4]. This is an important consideration given the strong prognostic value of VO_{2peak} as an indicator of cardiovascular mortality and cardiometabolic health in general [5], with the American

[1]Mitochondrial and Neuromuscular Disorders Unit, Vall d'Hebron Institut de Recerca, Universitat Autònoma de Barcelona, Barcelona, Spain [2]Centro de Investigación Biomédica en Red de Enfermedades Raras (CIBERER), Madrid, Spain [3]Universidad Pablo de Olavide, Sevilla, Spain [4]Grup de Recerca en Malalties Neuromusculars i Neuropediàtriques, Department of Neurosciences, Institut d'Investigacio en Ciencies de la Salut Germans Trias i Pujol i Campus Can Ruti, Universitat Autònoma de Barcelona, Badalona, Spain [5]Physical Activity and Health Research Group ('PaHerg'), Research Institute of the Hospital 12 de Octubre ('imas12'), Madrid, Spain [6]EATRIS, European Infrastructure for Translational Medicine, Amsterdam, Netherlands [7]Mitochondrial and Neuromuscular Diseases Laboratory, 12 de Octubre Hospital Research Institute (i+12), Madrid, Spain [8]Copenhagen Neuromuscular Center, Department of Neurology, Rigshospitalet, University of Copenhagen, Copenhagen, Denmark [9]Faculty of Sport Sciences, European University, Madrid, Spain [10]Centro Andaluz de Biología del Desarrollo, Universidad Pablo de Olavide, Sevilla, Spain

[11] Both authors contributed equally to this work.

*Corresponding author. Departament de Patologia Mitocondrial i Neuromuscular, Hospital Universitari Vall d'Hebron. Institut de Recerca (VHIR), Barcelona, Spain. Tel.: +34934894057. E-mail: tomas.pinos@vhir.org (T. Pinós).

**Corresponding author. Tel.: +4535457614. E-mail: thomas.krag@regionh.dk (T.O. Krag).

Received October 7, 2022 • Revision received November 14, 2022 • Accepted November 24, 2022 • Available online 28 November 2022

Heart Association recently advocating for the routine assessment of this measure as a clinical vital sign [6]. In this effect, recent data from the European registry of patients with McArdle disease (EUROMAC; http://www.euromacregistry.eu) indicate an overall unhealthy cardiometabolic profile for these individuals, with two-thirds showing high body mass index values and ~12% having cardiovascular disease (8% with coronary artery disease) despite the relatively young age of the cohort (median age 46 years) [7]. The finding of a low VO_{2peak} in patients has been replicated in the genetically manipulated mouse (knock-in) model of McArdle disease that we previously generated—harboring the commonest *Pygm* genotype (p.R50*/p.R50*) that causes the disorder in Caucasians—and which muscle phenotype mimics that of affected patients, thereby representing an accurate study model [7,8]. Indeed, the aerobic fitness of McArdle mice is also much lower compared to wild-type (WT) controls [9].

At the mechanistic level, the low VO_{2peak} of patients with McArdle disease has been traditionally associated with a reduced flux of substrates through the glycolytic pathway, thereby impairing oxidative metabolism—as reflected for instance by slow oxygen uptake kinetics during the transition from rest to exercise [10], or slow rate of phosphocreatine recovery following exertion [11]. Indeed, the production of pyruvate, a molecule that plays an anaplerotic role in the Krebs cycle, is reduced in patients [12], with intravenous glucose administration increasing VO_{2peak} (by about 20%) and muscle oxidation [13]. On the other hand, not only impaired glycolytic flux, but also functional impairment of oxidative metabolism in muscle fibers—as reflected by a slow recovery of muscle ADP after brief ischemic exercise exercise—has been described in McArdle patients [14]. In this context, other potential variables related to the structure/function of the cell organelles that are responsible for aerobic energy provision, mitochondria, could explain—at least partly—the low VO_{2peak} that characterizes this disease, with previous data indeed showing that the muscle levels of citrate synthase (CS), a key mitochondrial enzyme that reflects the function of this organelle, is lower in McArdle mice than in WT controls [15].

Mitochondria form a branched tubular network, with a balance between the fusion and fission of these organelles needed not only to ensure integrity of this network but also maintenance of normal levels of mitochondrial membrane potential and respiration [16]. On the other hand, in mammals, VO_{2peak} is associated with skeletal muscle mitochondrial respiration [17] and is linearly related with total mitochondrial volume and surface area [18]. In this context, it might be hypothesized that the massive intracellular glycogen deposits associated with McArdle disease—i.e., 27-fold higher in McArdle than in WT mice—due to the inherited block in glycogenolysis could alter the normal cytoskeleton structure of skeletal muscle fibers and thus their mitochondrial tubular network [19]. In turn, because IIA and IIX fibers are more structurally affected (i.e., 'degenerated') than type I and IIB fibers in McArdle mice [20,21], the mitochondrial tubular network could also be differently affected based on the relevant muscle phenotype (*i.e.*, with a predominance of either IIA or IIX fibers, respectively).

The aim of this study was to determine whether mitochondrial network integrity and function is altered in skeletal muscle fibers in the context of McArdle disease. To this purpose, we used the mouse model of this condition as well as skeletal muscle biopsies from patients. If mitochondrial network integrity and function were actually altered, this would help to explain, at least partly, the major impairment in muscle oxidative metabolism that characterizes this disease. In addition, we aimed to provide corroborating, strong evidence for an impaired VO_{2peak}—well below normative values—in the longest series of patients studied to date.

2. MATERIAL AND METHODS

2.1. Ethical approval

All experimental procedures in mice were approved by the relevant institutional review board (vall d'Hebron hospital, barcelona, Spain; protocol number 58/17 CEEA; 35/04/08) and were conducted in accordance with the European Convention for the Protection of Vertebrate Animals used for Experimental and Other Scientific Purposes (ETS1 2 3) and Spanish laws (32/2007 and R.D. 1201/2005). The study in humans adhered the ethics guidelines of the Declaration of Helsinki, and was approved by the Ethics Committee of Hospital 12 de octubre, madrid, Spain (reference 16/081). All participants were informed about the study procedures and provided written informed consent

2.2. Patients' muscle biopsies

Biopsies were taken with a Bergstrøm needle from two patients, patient 1 a male age 61 years with proximal weakness and patient 2 one female age 34 years, both homozygous for the pathogenic p.50* variant in the *PYGM* gene.

2.3. Studies in mice

Previously developed p. R50*/p.R50 × mice, back-crossed for 10 generations to C57/6 J background, were used in this study [19,22]. Cohorts of 10 wild-type (WT) and McArdle mice (male and female, aged between 8 and 20 weeks) were studied. All mice were sacrificed by cervical dislocation immediately before dissection of the hind-limb muscles (*i.e.* gastrocnemius, quadriceps, and *tibialis* anterior [TA]).

2.4. Histochemistry

Dissected muscles were flash frozen in isopentane cooled in liquid nitrogen and stored at −80 °C until analysis. Twelve μm cryosections were stained with hematoxylin and eosin (H&E) for general histopathological evaluation as previously described [19]. Glycogen content was analyzed with periodic acid—Schiff (PAS) staining by sequentially incubating the sections with periodic acid (Fisher Scientific; Hampton, NH) (0.5%) for 5 min, water wash, Schiff 's solution (Merck-Millipore; Burlington, MA) for 15 min, water for 1 min, alcohol-xylol dehydration, and DPX mounting (Sigma—Aldrich; St. Louis, MO). Myophosphorylase activity staining was performed by incubating muscle sections for 45 min with a solution containing 1% glucose-1-phosphate, 0.2% AMP, and 0.02% glycogen in 0.1 M sodium acetate buffer, pH 5.6. Sections were washed with water, Lugol's iodine was applied for 3 min and samples were mounted with Aquatex. Staining for succinyl dehydrogenase (SDH) was done as by incubating cryosections in 0.1 M PBS and 0.1 M succinate with 1 mg/ml nitro blue tetrazolium (all Merck-Millipore) for 2 h at 37 °C followed by water wash, alcohol dehydration and mounting with Pertex (Sakura, Alphen aan den Rijn, The Netherlands). Cytochrome c oxidase (COX) activity staining was performed in cryosections as previously described [23]. Staining for myosin heavy chain type II (fast) was done by incubating cryosections with antibody (Leica Biosystems, Nussloch, Germany) for an hour at room temperature, followed by washing and incubating in secondary antibody and development with 3,3′-diaminobenzidine (DAB) according to manufacturer's instructions (Agilent, Santa Clara, CA).

2.5. Immunofluorescence

Formalin fixed paraffin-embedded quadriceps and TA muscles from WT and McArdle mice and OCT embedded frozen quadriceps biopsies from patients were used. Muscle samples were blocked in buffer (3% fetal calf serum in PBS) prior to staining. For the studies of

cytoskeleton, mitochondrial network and dynamics, and fiber type, sections were stained with the relevant antibodies (**Supplementary File 1**). Finally, sections were stained with 4′,6-diamidino-2-phenylin- dole (DAPI) nucleic acid stain reactive (Invitrogen; Carlsbad, CA), for 5 min and mounted with ProLongTM Gold Antifade reagent (Molecular probes; Eugene, OR). Images were taken using a Leica DM-IRB inverted microscope (Leica Microsystems; Wetzlar, Germany) and a Zeiss LSM980 fully-spectral confocal microscope with AiryScan 2 confocal super-resolution detector (Zeiss Microscopy; Jena, Germany). Super-resolution images were analyzed with the Zeiss-ZEN software (Zeiss Microscopy).

2.6. Electron microscopy

To visualize the ultrastructure of mitochondria, we used electron microscopy. Briefly, a McArdle mouse was perfused with 2% EM-grade glutaraldehyde in 0.05 M phosphate buffer (Sigma—Aldrich), the TA was dissected, and a piece was cut from the muscle. From patients, a small piece of muscle biopsy was incubated in the same buffer as the mouse was perfused with for 48 h at 4°. Muscle pieces from mice and patients were then rinsed in 0.15 M sodium cacodylate buffer (Sigma—Aldrich) for 30 min, and postfixed in 2% osmium tetraoxide (Polysciences Inc., Warrington, PA) in 0.05 M potassium ferrocyanide (K4Fe [CN]6) (Sigma—Aldrich) overnight at 4 °C, rinsed for 3 × 10 min in distilled water, stained with 1% uranyl acetate in distilled water for 1 h before 3 × 10 min rinse in water before graded dehydration in ethanol, followed by graded infiltration with propylene oxide and Epon (TAAB Laboratories Equipment Ltd., Aldermaston, UK). The sample was embedded in 100% Epon overnight followed by polymerization at 60 °C for 24 h. After postfixation, the fibers were rinsed twice in 0.1 M sodium cacodylate buffer at 4 °C, dehydrated through a graded series of alcohol at 4 to 20 °C, infiltrated with graded mixtures of propylene oxide and Epon at 20 °C, and embedded in 100% Epon at 30 °C. Ultrathin sections were cut from the transversely oriented muscle using a Leica EM UC7 ultramicrotome (Leica Microsystems) and contrasted with uranyl acetate and lead citrate (Leica Microsystems). Sections were visualized in a CM100 transmission electron microscope (Philips; Amsterdam, The Netherlands), fitted with a 4-Mpixel Veleta camera (Olympus Soft Imaging Solutions GmbH; Munster, Germany). Image acquisition was done using iTEM software (Olympus Soft Imaging Solutions GmbH).

2.7. Mitochondrial DNA copy number

Total DNA was extracted from TA and quadriceps muscles from WT and McArdle mice using the QIAamp DNAMini Kit (Qiagen; Hilden, Germany). Mitochondrial DNA (mtDNA) copy number was determined by real-time PCR, as previously described [24], and expressed as the ratio between mitochondrially-encoded 16 S RRNA (*mtRNR2*) gene copy number and nuclear Angiogenin-1 (*Ang*) gene copy number, with *Ang* being a nuclear single-copy gene. Results are expressed as the mtDNA/nuclear DNA *(mtRNR2/Ang*) copy number ratio. The following Taqman fluorogenic probes were used: (i) *mtRNR2* gene (forward primer: 5′AATGGTTCGTTTGTTCAACGATT 3′; reverse primer: 5′ AGAAACCGACCTGGATTGCTC 3′; probe: FAM-5′ AAGTCCTACGTGATCTGAGTT 3′-MGB); (ii) *Ang* (Mm00833184_s1).

2.8. Mitochondrial DNA deletion

To determine the presence of mtDNA deletions, a long-polymerase chain reaction (PCR) was performed using the following primers: forward primer (nucleotide position 2473—2505 of the NCBI Reference Sequence: NC_005089.1) 5′-GGTTCGTTTGTTCAACGATTAAAGTCCTACGTG-3′; and reverse primer (nucleotide position 1953—1924 of the NCBI Reference Sequence: NC_005089.1) 5′-GAGGTGATGTTTTTGGTAAACAGGCGGGGT-3′. The PCR temperature cycling conditions were as follows: initial denaturation at 92 °C for 2 min; 30 cycles of denaturation at 92 °C for 2 min, and annealing/elongation at 68 °C for 12 min. The final cycle was followed by extension at 68 °C for 15 min. The PCR product was separated in a 0.8% agarose gel stained with ethidium bromide (Sigma) and visualized with the Gel Doc XR + System (Bio-Rad; Hercules, CA).

2.9. mRNA levels

Total RNA was obtained from quadriceps and TA muscles from WT and McArdle mice as previously described [25] following the manufacturer's instructions (TRIzol, Invitrogen). RNA was treated with DNase I, amplification grade (Invitrogen) to eliminate any DNA trace. Complementary DNA was synthesized from RNA using the high-capacity complementary DNA archive kit (Applied Biosystems, Foster City, CA), which uses random primers. We used real-time PCR, with TaqMan fluorogenic probes in a 7900 real-time PCR System (Applied Biosystems) to assess mRNA levels of the following genes in quadriceps and TA muscles: peroxisome proliferator activated receptor alpha (*Ppara*, Mm00440939_m1) and beta (*Pparb*, Mm00803184_m1), peroxisome proliferative activated receptor, gamma, coactivator 1 alpha (Mm01208835_m1) and beta (Mm00504730_m1), estrogen related receptor, alpha (Mm00433143_m1), mitochondrially encoded NADH:ubiquinone oxidoreductase core subunit 4 (*mtND4* [forward primer: 5′ TGCATCAATCATAATCCAAACTCCATGA 3′; reverse primer: 5′ GGCAGAATAGGAGTGATGATGTGA 3′: probe FAM-5′ CCGACATCA TTACCGGGTTTTCCTCTTG 3′-MGB]) and 16 S RRNA (*mtRNR2*) [forward primer: 5′ aatggttcgtttgttcaacgatt 3′; reverse primer: 5′ agaaaccgacctggattgctc 3′; probe: FAM-5′ aagtcctacgtgatctgagtt 3′-MGB]). Results were normalized to peptidylprolyl isomerase A (*Ppia*) gene mRNA levels (probe Mm02342430_g1) and quantified using 7900 SDS v2.4.1 software (Applied Biosystems).

2.10. Western blots

Muscle samples from gastrocnemius, quadriceps, and TA muscles from WT and McArdle mice were homogenized using Pellet pestles Cordless motor (Sigma—Aldrich) in cold homogenization buffer (Tris—Hcl 20 mM, NaCl 150 mM and Triton ×100 1%) and centrifuged (10,000 g) for 10 min at 4 °C. The samples were placed in boiling water for 3 min, before 30 μg of protein was applied to each lane. Unspecific binding sites on the blots were blocked by incubation in 5% low-fat dried milk powder in a phosphate buffered saline. Membranes were incubated in primary antibodies overnight at 4 °C (**Supplementary File 1**) and in secondary antibodies for 3 h at room temperature. Ponceau S and Amido Black staining solutions (both from Sigma—Aldrich) were used as a loading control for all the membranes. Membranes were developed with Immobilon Western Chemiluminiscent HRP Substrate (Merck-Millipore) and images obtained with a LICOR Odyssey® Fc Imaging System (LICOR Biosciences; Lincoln, NE) and quantified with Image Studio™ Lite software, version 5.2 (LICOR Biosciences).

2.11. Mitochondrial oxidative phosphorylation system

150 mg of gastrocnemius, quadriceps and TA muscle samples from WT and McArdle mice were resuspended in 200 μl mannitol buffer, pH 7.2 (mannitol 225 mM, sucrose 75 mM, Tris—HCl 10 mM and EDTA 0.1 mM), and sonicated during 5 s at moderate intensity to obtain a homogenous solution. Protein content was determined using Coomassie Plus protein assay reagent (Pierce; Rockford, IL), adjusting the solution with mannitol buffer to a final protein concentration of 2 mg/

ml. Mitochondrial respiratory complex (C) I, II, and IV, and CS activities were determined as previously described [26].

2.12. Mass spectrometry

150 mg of quadriceps tissue from WT and McArdle mice were homogenized using mortar and pestle and resuspended in 10 mM K_2HPO_4 (100 μL) and 10 volumes of chilling (−20 °C) 60% methanol were added. Then samples were sonicated three times for 20 s with 1 min incubation on ice between cycles. Sonicated samples were incubated on ice for 10 extra min and centrifuged at full speed (17,000 g) in a refrigerated (4 °C) microcentrifuge. Supernatant was filtered using nylon 0.2 μm microfilters and dryer under nitrogen stream to preserve oxygen-free atmosphere. Dried samples were conserved in ultra-freezer (−80 °C) until further use. For NAD/NADH determination dried samples were reconstituted in 50 μL mobile phase solvent A. UPLC separation was carried out using a gradient of acetonitrile (solvent A 5% acetonitrile in 10 mM ammonium carbonate, solvent B 95% acetonitrile in 10 mM ammonium carbonate). The two-step gradient consisted in a smooth ramp (initial 5%B raising to 60%B in min 7.5) followed by a 2 min ramp to wash all retained analytes (min 9.5, 100%B). Washing conditions were sustained for 1 min (min 10.5) and initial conditions were restored (min 13.5). Column was re-equilibrated for 5 additional min before next injection cycle. Separation was achieved using an I-Class Waters UPLC equipped with Acquity BEH Amide 1.7 μm 2.1 × 50mm column (Waters, cat#186004800). Nucleotides were detected using a single-quadrupole Waters QDA ESI MS (probe 500 °C, 800 V ionization needle, −15 V collision energy, SIR channels 664 and 666 *m/z*). Analytical standards for NAD+/NADH were used for UV-Vis spectral confirmation and elution time (spiked samples).

For pyruvate, lactate and glucose-6-phsophate MS SIR channels were set to 111, 90 and 260 *m/z* respectively (probe 500 °C, 800 V ionization needle, 20 V collision energy). Analytical standards of these metabolites were used for MS confirmation and elution time (spiked samples).

2.13. Peak oxygen uptake in patients

The patients and their controls were assessed from January 2011 to December 2018 in the exercise physiology laboratory of the Universidad Europea de Madrid (UEM). Inclusion criteria for both patients and controls were being free of any major cardiorespiratory disease or severe condition contraindicating exercise. In patients (all identified in the Spanish registry of patients [27]), diagnosis of McArdle disease was ascertained by the identification of a documented pathogenic mutation in both alleles—whether in homozygosity or compound heterozygosity—of the *PYGM* gene (**Supplementary File 2**). All the tests were performed using the same cycle-ergometer (Ergoselect 220 KL, Ergoline GmbH; Bitz, Germany) and metabolic cart (Vmax 29C, Sensormedics Corp.; Yorba Linda, CA), The maximum test was preceded by a 5-min free-wheel pedaling warm-up, after which the workload was increased following a ramp protocol (10 [patients] or 20 W/min [control]s) until volitional exhaustion (9). The VO_{2peak} was determined as the highest VO_2 value (20-second average) recorded during the tests. All the tests were supervised by the same researchers (AL, AS, CFL).

2.14. Statistical analyses

In McArdle mice, to analyze the relevant genotype effect in normally distributed values, a Student t-test was applied, whereas the non-parametric Mann—Whitney U-test was used when values were not normally distributed. The Shapiro—Wilk normally test was used to check whether the analyzed data followed a normal distribution. The mean VO_{2peak} values of patients and controls (men and women separately) were compared with the Student's t test for unpaired data. The level of significance was set at 0.05 for all statistical analyses.

3. RESULTS

3.1. Structural damage, glycogen levels and mitochondrial content

In order to elucidate whether mitochondrial structure and function is affected in the different fiber types from the skeletal muscle of McArdle mice, we first performed an in-depth histopathologic analysis. H&E staining showed muscle fibers in disarray, of varying sizes, as well as the presence of large intra-fiber voids and some centrally-nucleated fibers (Figure 1A i-ii) [20,21]. Also characteristic was the intense positive PAS staining, reflecting large glycogen accumulation, with some fibers accumulating more glycogen than others (Figure 1A iii-iv, yellow and black arrows). Amylase treatment reduced glycogen content to normal levels (Figure 1A v), indicating that the accumulated glycogen had normal structure. Myophosphorylase staining in WT mice showed different intensities depending on fiber type, being more intense in smaller fibers (*i.e.*, usually more oxidative**,** Figure 1A vi, yellow and black arrows). As expected, myophosphorylase staining was null in the muscle fibers of McArdle mice (Figure 1A vi). This differential degree of myophosphorylase staining in WT suggests differential glycogen disposal among fiber types. Interestingly, those fibers with higher SDH and COX activity staining as well as cytochrome c oxidase subunit II (COX II) and voltage-dependent anion channel (VDAC) immunodetection were the ones showing the most affected morphology in McArdle mice, with larger intra-fiber voids (**Figure 1**A vii-x). Additionally, SDH activity and PAS staining in muscle consecutive sections showed that fibers with larger glycogen depots were those with higher SDH activity (Figure 1A xi-xii). Furthermore, immunofluorescence staining against COX II and VDAC mitochondrial proteins showed differential distribution of subcellular mitochondria in WT and McArdle mice (**Supplementary File 3A**). Using specific antibodies against the different fibers types we observed that type I and IIX/IIB fibers were less structurally damaged than IIA, IIA/IIX and IIX fibers in the skeletal muscle of McArdle mice (Figure 1A xiii-xv). In addition, double immunostainings of COX II with myosin heavy chain (MHC) type I, IIA or IIB showed that IIA fibers had higher COX II staining intensity than type I and IIB fibers (Figure 1A xvi-xviii), with higher VDAC staining observed in IIA and IIX fibers (**Supplementary File 3B**). Finally, triple fiber type immunostaining and PAS staining in consecutive muscle sections showed that IIA and IIX fibers accumulated more glycogen than IIB fibers (Figure 1A xix and xx).

Overall, the aforementioned results would support that the most degenerated muscle fibers in the McArdle mouse model are those with higher glycogen and mitochondrial contentthat is, type IIA and IIX fibers. Therefore, the next step was to assess whether mitochondrial integrity was conserved in these highly affected muscle fibers. In this effect, electron microscope images showed the presence of abnormally large mitochondria that had lost—whether partially or totally—their cristae (with rupture and discontinuation of the inner and outer membranes) or were thoroughly degenerated (Figure 1B). The most structurally damaged mitochondria were those surrounded by glycogen particles (Figure 1B). Besides the altered morphology, mitochondria had also lost their normal regular distribution in the intermyofibrillar space along both the A band and Z line (**Supplementary File 3C**).

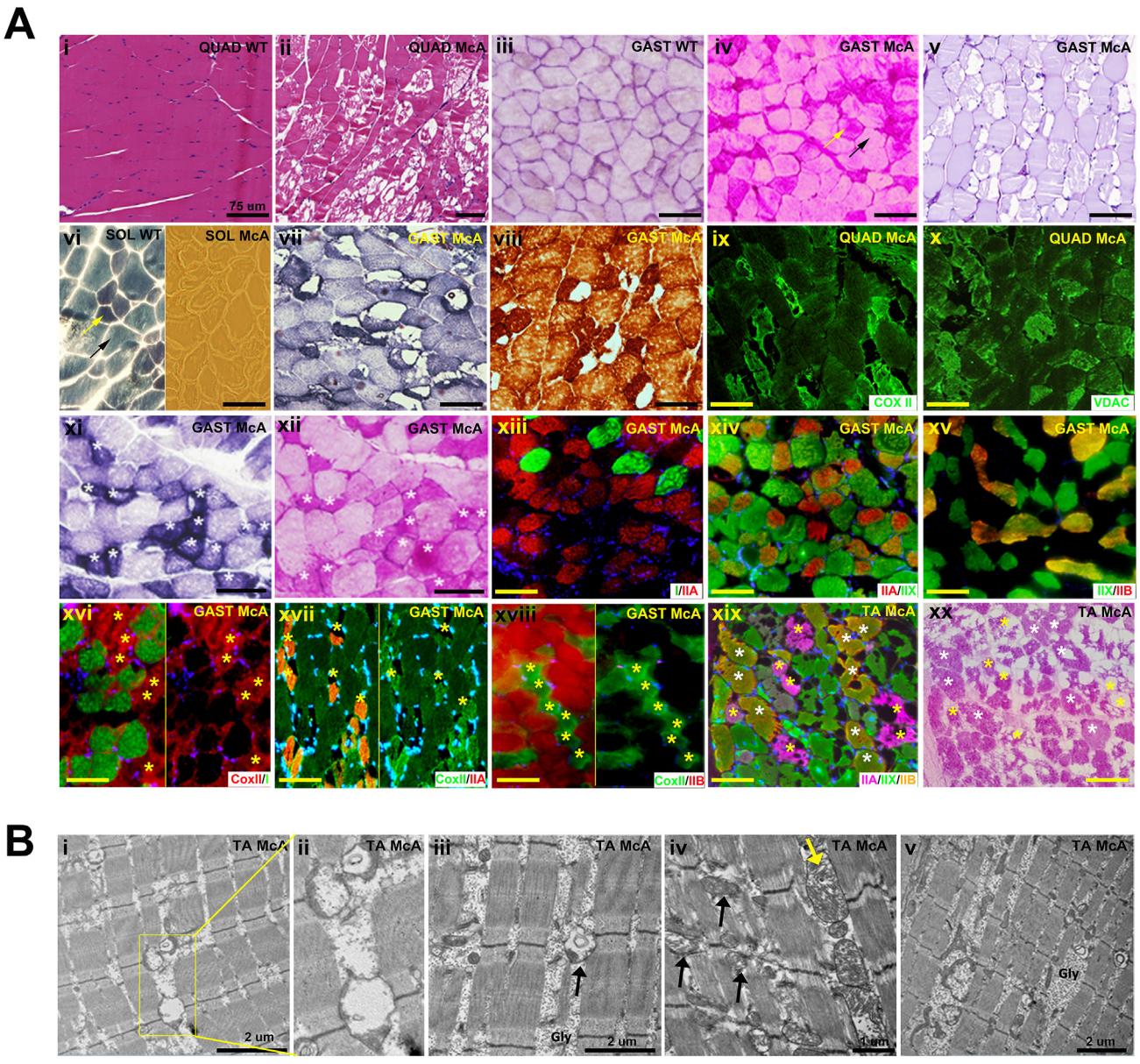

Figure 1: Histopathological analysis of the skeletal muscle from the McArdle (p.R50*/p.R50* *Pygm*) mouse model. (A) Histochemical, immunohistochemical and immunofluorescence analysis of the skeletal muscle from McArdle mice**; i)** and **ii)** H&E staining in the quadriceps from wild-type and McArdle mice; **iii)** and **iv)** PAS staining in the gastrocnemius from wild-type and McArdle mice; **v)** PAS-Diastase staining in the gastrocnemius from McArdle mice; **vi)** Myophosphorylase activity staining in the soleus from wild-type and McArdle mice; **vii** and **viii)** SDH and COX activity staining, respectively, in the gastrocnemius from McArdle mice; **ix)** and **x)** COXII and VDAC immunofluorescence, respectively, in the quadriceps from McArdle mice; **xi)** and **xii)** SDH activity and PAS staining, respectively, in gastrocnemius serial sections from McArdle mice; white asterisks show those fibers with high SDH activity and PAS staining; **xiii)** immunofluorescence showing type I (green) and IIA (red); **xiv)** type IIA (red) and IIX (green); and **xv)** type IIX (green) and IIB (red) muscle fibers in the gastrocnemius from McArdle mice; **xvi)** immunofluorescence staining for COXII (red) and type I fibers (green) in the gastrocnemius from McArdle mice, with yellow asterisks marking the same fibers with and without type I fiber staining; **xvii)** immunofluorescence staining for COXII (green) and type IIA fibers (red) in the gastrocnemius from McArdle mice, with yellow asterisks marking the same fibers with and without type IIA fiber staining; **xviii)** immunofluorescence staining for COXII (green) and type IIB fibers (red) in the gastrocnemius from McArdle mice, with yellow asterisks marking the same fibers with and without type IIB fiber staining; **xix)** immunofluorescence staining showing type IIA (pink), IIX (green), IIB (orange) muscle fibers, and DAPI (the nuclei, blue) in the tibialis anterior muscle of McArdle mice; and **xx)** consecutive serial section from (**xix**) stained with PAS; for **xix)** and **xx)** yellow asterisks mark muscle fibers with more intense PAS staining while white asterisks mark muscle fibers presenting less intense PAS staining. All scale bars correspond to 75 μm. **(B)** Electronic microscopy analysis of the ultrastructure integrity of mitochondria in the skeletal muscle of McArdle mice (TA). Z-line mitochondria are indicated with black arrows, while A-band mitochondria are shown with a yellow arrow. Scale bars correspond to 1 or 2 μm as indicates. **Abbreviations**; QUAD: quadriceps; GAST: gastrocnemius; SOL: soleus; TA: tibialis anterior; WT: wild-type; McA: McArdle; Gly: glycogen.

Thereafter we aimed to assess whether the observed loss of mitochondrial integrity in those fibers with higher glycogen content was associated with mitochondrial network disruption, with the results shown below.

3.2. Mitochondrial network

VDAC fluorescent staining showed massive alteration of the mitochondrial network both along the A band and across the Z line in McArdle mouse muscles (Figure 2A). Additionally, fragmented

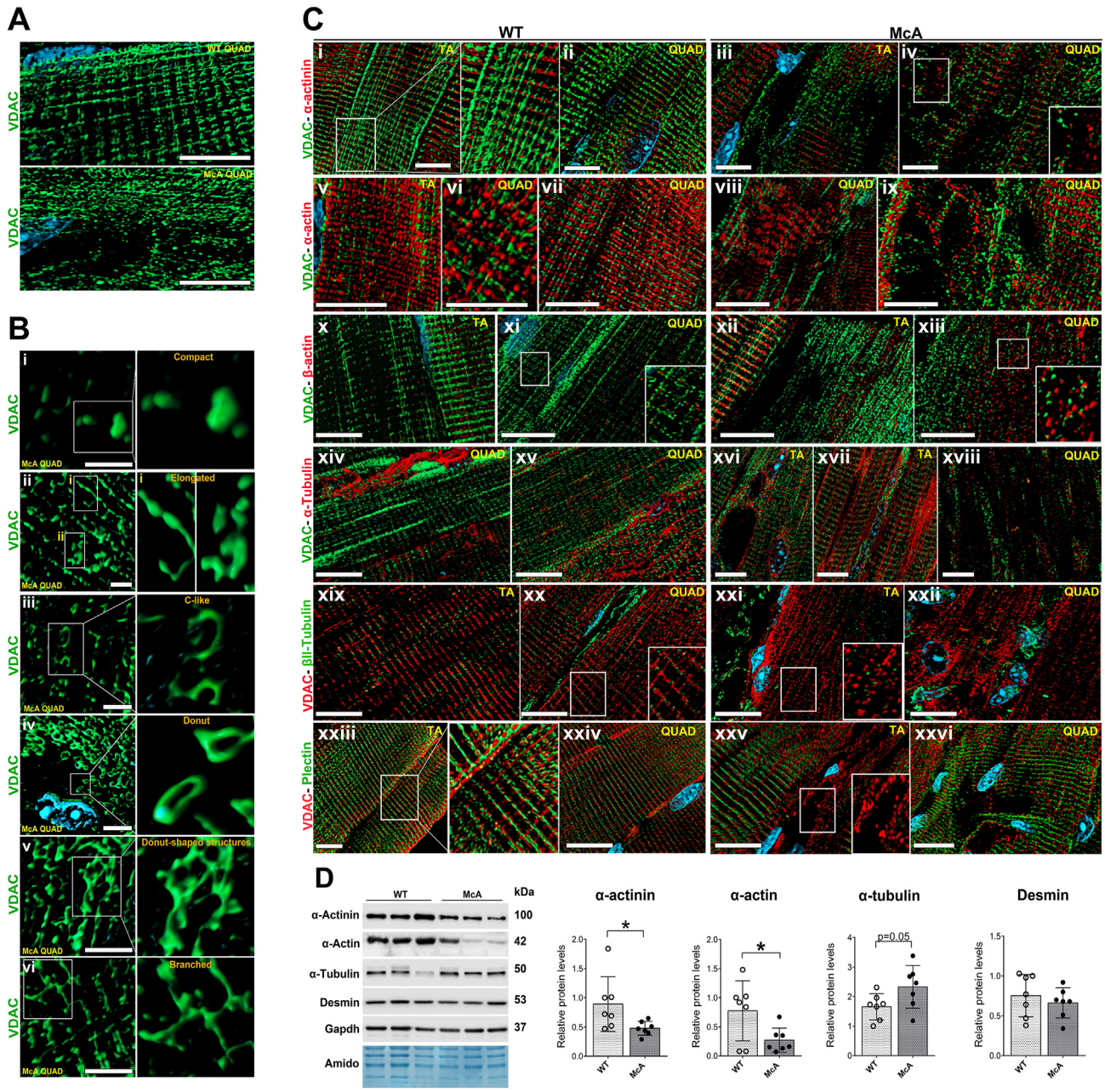

Figure 2: Cytoskeleton and mitochondrial network integrity analysis in the skeletal muscle from the McArdle (p.R50*/p.R50 × *Pygm*) mouse model. (A) VDAC immunofluorescence analysis of mitochondrial network. Scale bars correspond to 25 μm. (B) Mitochondrial morphology analysis showing different mitochondrial sizes and shapes in McArdle mice; squared regions are magnified and shown in detail. Scale bars correspond to 5 μm. (C) Immunofluorescence analysis of the cytoskeleton and mitochondrial network integrity in the skeletal muscle from wild-type and McArdle mice; wild-type (i-ii) and McArdle mice (iii-iv) immunofluorescence staining of VDAC (green) and α—actinin (red); loss of α—actinin staining is clearly visible in (iii-iv), while a complete disruption of the mitochondrial network and cytoskeleton is shown in the square box in (iv). Wild-type (v-vii) and McArdle mice (viii-ix) immunofluorescence staining of VDAC (green) and α—actin (red); irregular A-band length is visible in (viii), while disrupted actin microfilaments and/or non-polymerized α—actin monomers are shown in (ix). Wild-type (x-xi) and McArdle mice (xii-xiii) immunofluorescence staining of VDAC (green) and β—actin (red); a complete disruption of the mitochondrial network and β—actin cytoskeleton structures is observed in (xii-xiii); the square box region shows isolated mitochondria and actin monomers. Wild-type (xiv-xv) and McArdle mice (xvi-xviii) immunofluorescence staining of VDAC (green) and α-tubulin (red); subsarcolemmal, as well as longitudinal and transversal interaction of microtubules with mitochondria is observed in (xiv-xv), while microtubules surrounding fiber voids and central nucleated fibers, aggregated in thick tubulin bundles or completely disrupted and/or non-polymerized are shown in (xvi-xviii). Wild-type (xix-xx) and McArdle mice (xxi-xxii) immunofluorescence staining of VDAC (red) and βII-tubulin (green); βII-tubulin aggregates in fiber voids (xxi) or surrounding centrally nucleated fibers (xxii) are observed, while irregularly dispersed βII-tubulin staining non co-localizing with mitochondria is observed in the square box (xxi). Wild-type (xxiii-xxiv) and McArdle mice (xxv-xxvi) immunofluorescence staining of VDAC (red) and plectin (green); regions surrounding fiber voids with no plectin staining are shown in (xxv-xxvi); completely disrupted mitochondrial network with the presence of isolated compact mitochondria can be seen in the square box in (xxv). All scale bars correspond to 25 μm. (D) Western blot analysis of cytoskeleton protein levels in the quadriceps from wild-type and McArdle mice (N = 7 (3 male) in both groups). As all the data followed a normal distribution according to the Shapiro—Wilk normally test, the Student's *t*-test was applied in all cases. Asterisk correspond to $p < 0.005$ in the statistic test. Abbreviations: VDAC: voltage-dependent anion channel; QUAD: quadriceps; TA: tibialis anterior; WT: wild-type; McA: McArdle; Gapdh: Glyceraldehyde-3-phosphate dehydrogenase; Amido: Amido black staining.

mitochondrial structures as well as isolated mitochondria showed a wide variety of shapes and size associated with network disruption. Among these, "compact", elongated, branched as well as c-shaped or "donut" like mitochondria—with this type of alterations previously shown to be associated to cellular stress [28,29]—were commonly observed close to large fiber voids (glycogen depots) (Figure 2B).

3.3. Cytoskeleton and mitochondrial network in McArdle mice

In a subsequent step we aimed to determine whether mitochondrial network disruption was associated with disarray of the cytoskeleton structure, as connections between the cytoskeleton and mitochondria are very important for the positioning of mitochondria within the cell [30]. In this regard, different cytoskeletal proteins comprising intermediate filaments (plectin and desmin), microtubules (α and βII-tubulin), actin microfilaments (α and β-actin) as well as the sarcomere (α-actinin-3) were analyzed by immunofluorescence, along with the mitochondrial protein VDAC. In WT mice, the different sarcomeric and cytoskeleton proteins showed a normal disposition in all muscle fibers, and VDAC staining indicated the presence of an intact mitochondrial network throughout the entire longitudinal and transversal axis of muscle fibers (Figure 2C). By contrast, in the skeletal muscle fibers from McArdle mice the cytoskeleton was especially disrupted in regions with large fiber voids—including myofibrils in disarray presenting loss of α-actinin-3 staining, actin microfilaments with irregular A-band length, regions enriched with non-polymerized α, β-actin as well as α-tubulin monomers (Figure 2C and Supplementary File 4A), aggregation of thick tubulin bundles nearby fiber voids (Figure 2C and Supplementary File 4A), irregularly dispersed βII-tubulin throughout the sarcolemma (sometimes distant from any mitochondrion) forming clusters within fiber voids or aggregates surrounding central nucleated fibers, and areas devoid of plectin and desmin staining (Figure 2C and Supplemnetary File 4B), along with the loss of transverse and longitudinal mitochondrial network. Interestingly, mitochondria and microtubules were intertwined forming a helicoid-like structure (**Supplementary File 4A,** white arrowheads) that in the case of McArdle mice could help to generate tension in order to maintain together the disrupted mitochondrial network fragments. Additionally, in the skeletal muscle fibers of McArdle mice some microtubules crossed through the holes of the "donut"-like mitochondria (**Supplementary File 4A**, yellow arrowheads).

Western Blot protein quantification showed that the cytoskeleton disruption in the muscle fibers of McArdle mice was accompanied by lower α-actinin-3 and α-actin protein levels, and a trend to higher α-tubulin protein levels (Figure 2D), possibly in an attempt to reorganize the entire cytoskeleton structure.

3.4. Mitochondrial fission/fusion proteins

It is known that disruption of the cytoskeleton structure and the mitochondrial network may alter mitochondrial fusion/fission dynamics [31,32]. Thus, we analyzed the fission-related proteins dynamin-related protein 1 (Drp1) and mitochondrial fission 1 protein (Fis1), and the fusion proteins mitofusin 2 (Mfn 2) and optic atrophy 1 (Opa 1) by immunofluorescence. In WT mouse muscle, both fission proteins were found close to both Z-disc associated and subsarcolemmal mitochondria (Figure 3A and Supplementary File 5A and C) whilst the fusion proteins Mfn 2 and Opa 1 were localized at the level of Z-disc in intermyofibrillar mitochondria, subsarcolemmal mitochondria, and in the mitochondria associated with the A-band (Figure 3A and Supplementary File 5D). By contrast, in McArdle mouse muscle, Drp1 transitioned from Z-disc mitochondria in semi-preserved mitochondrial network structures, to its isolate localization within the sarcoplasm (**Supplementary File 5A**), and/or co-localizing with isolated (and enlarged) mitochondria (Figure 3A), suggesting the occurrence of mitochondrial fission events in fiber regions with a highly unstructured mitochondrial network; interestingly, fission-like events were also observed (**Supplementary File 5A and B**; white arrowheads), where α-tubulin immunofluorescence staining suggested that microtubules might help Drp1 to constrain mitochondria to drive scission (**Supplementary File 5B**; white arrowheads). Further analysis in McArdle mice revealed that Fis1 co-localized with VDAC staining in longitudinal mitochondrial aggregates (Figure 3A), or as in the case of Drp1, in fission-like events in fragmented mitochondrial structures (**Supplementary File 5C**, white arrowheads). In the case of fusion proteins, Mfn2 staining was more pronounced in mitochondria located in close proximity to fiber damage, central nucleated fibers, and large glycogen depots (Figure 3A), while Opa1 staining co-localized with isolated and dispersed mitochondria, as well as nearby regions of large glycogen depots and central nucleated fibers (Figure 3A). Interestingly, the staining of Mfn2 and Opa1 in McArdle mouse muscle did not entirely co-localize with that of mitochondria, especially in regions of fiber damage and regeneration (Figure 3A).

As Mfn2 has also been described to be localized in endoplasmic (ER)/sarcoplasmic reticulum (SR) membranes, we next wanted to assess whether the SR network was also disrupted in the skeletal muscle of McArdle mice and found that calsequestrin staining showed enlarged SR distribution in longitudinal bundles in comparison to WT animals (Figure 3A). On the other hand, no significant changes in the quantity of the fission proteins Drp1 and mitochondrial dynamics protein of 49 kDa (Mid49), as well as of the fusion-related protein Opa1, were found in the muscle of McArdle mice; in turn, these animals showed lower levels of Mfn2 fusion protein levels, suggesting an impairment in mitochondrial fusion (Figure 3B).

3.5. Mitochondrial content and biogenesis

As mitochondrial network and dynamics have been directly related to mitochondrial function, homeostasis and quality control, we next examined mitochondrial content and biogenesis in the skeletal muscle of McArdle mice [28,33]. Remarkably, lower mtDNA levels were found compared with WT animals (Figure 4A), albeit with no evidence of mtDNA deletions (Figure 4A). Additionally, lower levels of mitochondrial transcription factor A (Tfam) and nuclear respiratory factor (Nrf1) protein levels, as well as lower *mtND4*, *Pgc1a*, *Ppara*, *Pparb* transcript levels were also observed in the TA muscle of McArdle mice (Figure 4B—E), suggesting an impaired mitochondrial biogenesis. Remarkably lower levels of VDAC protein levels were also found in the gastrocnemius and quadriceps muscle of McArdle mice (Figure 4F), thereby suggesting an impairment in mitochondrial content. On the other hand, the protein levels of nuclear factor erythroid 2-related factor 2 (Nrf2) were significantly higher in the TA of McArdle mice with respect WT mice (Figure 4E). Nrf2 is a master regulator of the cellular redox homeostasis [34], with increased levels of this molecule likely reflecting an attempt to counterbalance mitochondrial ROS production derived from mitochondrial network disruption and dysfunction.

3.6. OXPHOS-related proteins

Lower levels of several OXPHOS-related proteins were observed in the skeletal muscle of McArdle mice compared to WT, as reflected both by lower Ndufa9 (complex I; CI) and CoxII (complex IV; CIV) protein levels in the quadriceps muscle, and lower complex III Uqcrc2 protein levels in the gastrocnemius muscle, respectively (Figure 5A). In order to

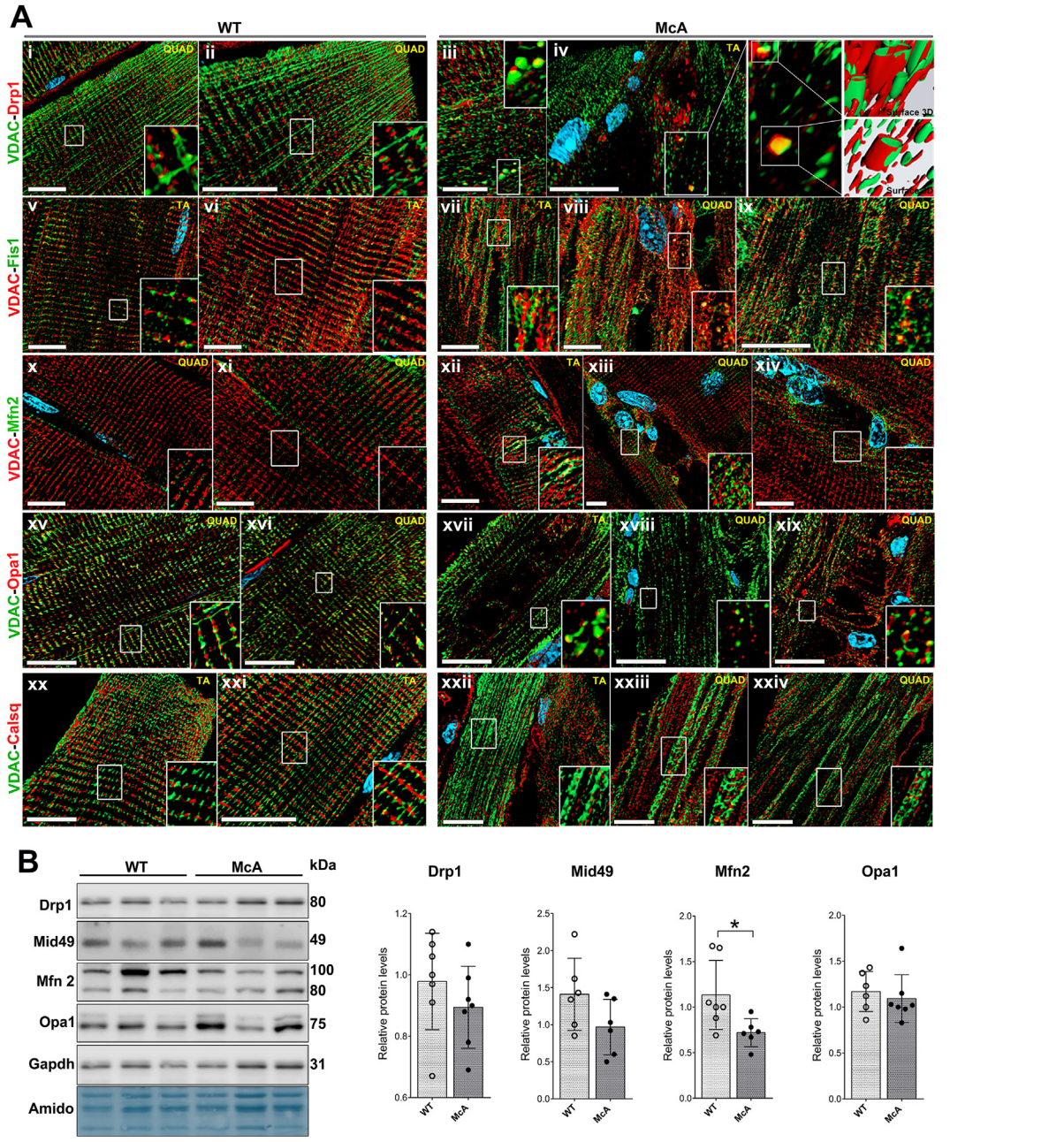

Figure 3: Altered subcellular localization of fission/fussion proteins in the skeletal muscle from the McArdle (p.R50*/p.R50 × *Pygm*) mouse model. (A) Immunofluorescence analysis of mitochondrial fission/fusion proteins in the skeletal muscle from McArdle mice. Wild-type (i-ii) and McArdle mice (iii-iv) immunofluorescence staining of VDAC (green) and Drp1 (red); Drp1 is observed in close proximity to mitochondria within the network in (i-ii), while Drp1 staining co-localizes with enlarged and isolated mitochondria in (iii-iv); square boxes show magnification of the Drp1-VDAC staining co-localization, while 3D Surface reconstruction images from the square box regions using the Zen-Blue software are also shown. Wild-type (v-vi) and McArdle mice (vii-ix) immunofluorescence staining of VDAC (red) and Fis1 (green); as with Drp1, Fis1 are found in close proximity of mitochondria within the network in (v-vi), while is found co-localizing with VDAC staining in longitudinal mitochondria aggregates in (vii-ix); square regions show magnification of the VDAC-Fis1 co-localization in the aggregates. Wild-type (x-xi) and McArdle mice (xii-xiv) immunofluorescence staining of VDAC (red) and Mfn2 (green); square boxes in (x-xi) show magnification of Mfn2 staining in close proximity of mitochondria in the Z-disc, while in (xii-xiv) show magnification of Mfn2 staining located in close proximity to fiber damage, central nucleated fibers, and large glycogen depots. Wild-type (xv-xvi) and McArdle mice (xvii-xix) immunofluorescence staining of VDAC (green) and Opa1 (red); in (xv-xvi) square boxes show co-localization of Opa1 in Z-disc mitochondria, while in (xvii-xix) square boxes show Opa1 co-localization with dispersed and isolated mitochondria. Wild-type (xx-xxi) and McArdle mice (xxii-xxiv) immunofluorescence staining of VDAC (green) and calsequestrin (red); enlarged calsequestrin distribution in longitudinal bundles in comparison to wild-type mice is observed in (xxii-xxiv). All scale bars correspond to 25 μm. (B) Western blot analysis of mitochondrial fusion and fission protein levels in the quadriceps from wild-type and McArdle mice (N = 6–7 (3 male) in both groups for the different variables). For Drp1 analysis, the Student's *t*-test was applied as data followed a normal distribution according to the Shapiro–Wilk normally test, whereas the Mann–Whitney *U*-test was used for Mid49, Mfn2 and Opa1. Asterisk correspond to $p < 0.005$ in the statistic test. Abbreviations: Drp1: Dynamin-related protein 1; Fis1: mitochondrial fission 1 protein; Mfn2: Mitofusin 2; Opa 1: optic atrophy protein 1; Calseq: calsequestrin; Mid49: mitochondrial dynamic protein of 49 kDa; QUAD: quadriceps; TA: tibialis anterior; WT: wild-type; McA: McArdle; Gapdh: Glyceraldehyde-3-phosphate dehydrogenase; Amido: Amido black staining.

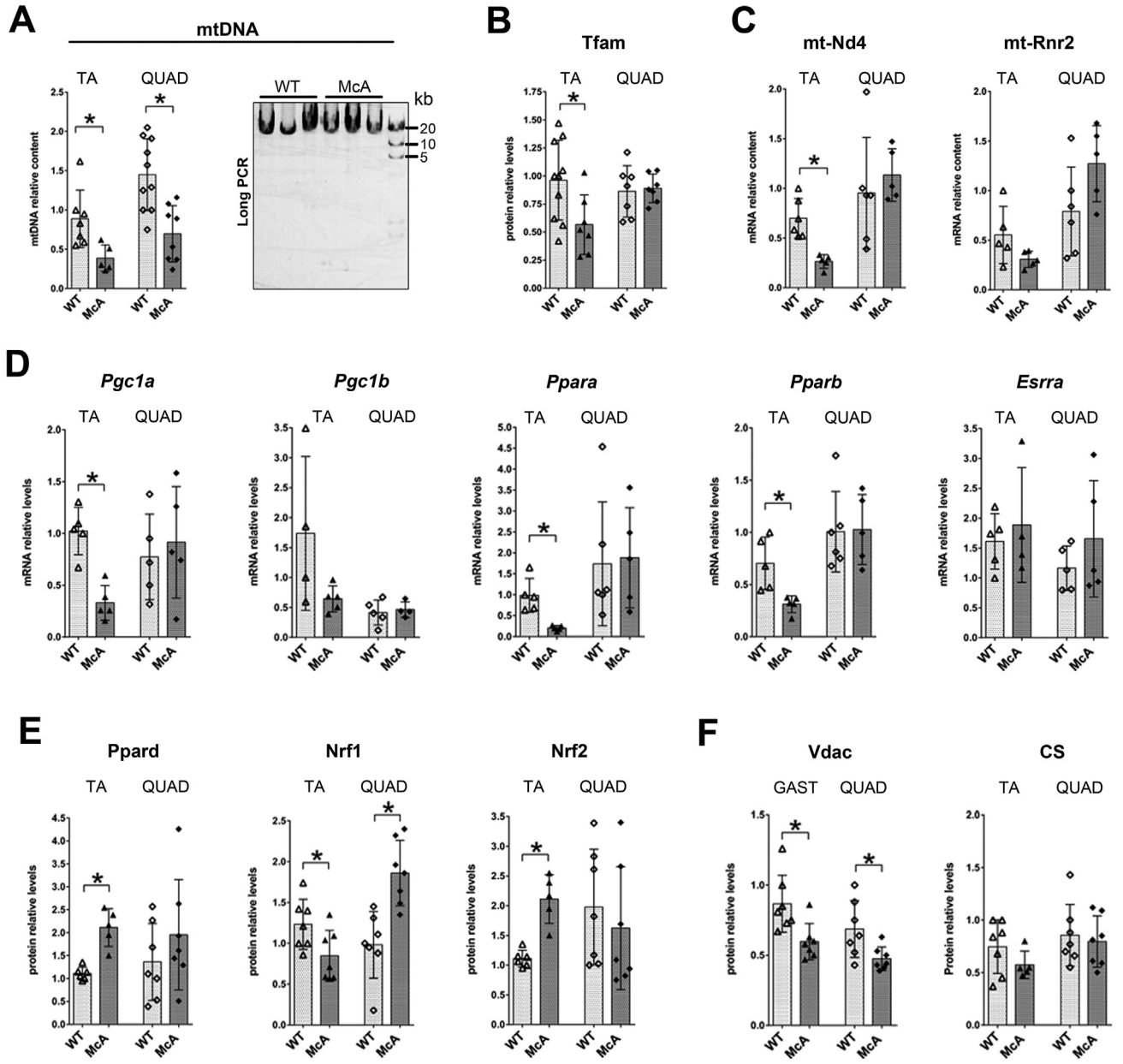

Figure 4: Analysis of mitochondrial biogenesis and content. (A) Analysis of mitochondrial DNA content (mtDNA) depletion in the tibialis anterior [N = 7 wild-type (71% male) and 5 McArdle mice (40% male)] and quadriceps [N = 10 wild-type (70% male) and 8 McArdle mice (63% male)] and deletions (in quadriceps) using qPCR and long PCR, respectively. **(B)** Western blot analysis of Tfam protein relative levels in tibialis anterior [N = 10 wild-type (50% male) and 7 McArdle mice (43% male)] and quadriceps [N = 7 wild-type (3 males) and 7 McArdle mice (3 males)]. **(C)** qPCR analysis of *mt—Nd4* and *mt-Rnr2* mRNA relative levels in tibialis anterior [N = 5—6 wild-type (3 males) and 5 McArdle mice (3 males)] and quadriceps [N = 5 wild-type (3 males) and 5 McArdle mice (3 males)]. **(D)** qPCR analysis of *Pgc1a*, *Pgc1b*, *Ppara*, *Pparb* and *Esrra* mRNA relative levels in the tibialis anterior [N = 4—5 wild-type (2—3 males) and 4—5 McArdle mice (2—3 males)] and quadriceps [N = 5—6 wild-type (50—60% male) and 4—5 McArdle mice (60—75% male)]. **(E, F)** Western blot analysis of Ppard, Nrf1, Nrf2, Vdac and CS protein relative levels in tibialis anterior [N = 6—7 wild-type (43—67% male) and 5—7 McArdle mice (29—40% male) and quadriceps (N = 7 (3 male) in both groups for the different proteins). When data followed a normal distribution (i.e. mtDNA quadriceps, Tfam, Ppard, Nrf1, Nrf2 quadriceps, VDAC and CS quadriceps protein levels) the Student's *t*-test was applied, whereas the non-parametric Mann—Whitney *U*-test was used for those (mtDNA tibialis anterior, *mt—Nd4*, *mt-Rnr2*, *Pgc1a*, *Pgc1b*, *Ppara*, *Pparb*, *Esrra* mRNA levels and Nrf2 and CS tibialis anterior protein levels) that were not normally distributed. Asterisks correspond to $p < 0.005$ in the statistic tests. **Abbreviations**: QUAD: quadriceps; TA: tibialis anterior; WT: wild-type; McA: McArdle; Tfam: transcription factor A, mitochondrial; mt—Nd4: mitochondrially encoded NADH:Ubiquinone oxidoreductase core subunit 4; mt-Rnr2: mitochondrially encoded 16 S rRNA; Pgc1a and b: PPARG Coactivator 1 alpha and beta; peroxisome proliferator activated receptor alpha and beta; Esrra: estrogen related receptor alpha; Nrf1: nuclear respiratory factor 1; Nrf2: nuclear factor erythroid 2-related factor 2; Vdac: voltage-dependent anion channel; CS: citrate synthase.

determine whether mitochondrial network disruption affected mitochondrial OXPHOS complex activities, the enzyme activity of CI, CII and CIV was measured in total muscle homogenates from gastrocnemius, TA and quadriceps, with the results showing significantly lower levels of CI and CIV activities in the gastrocnemius of McArdle mice vs WT controls (Figure 5B).

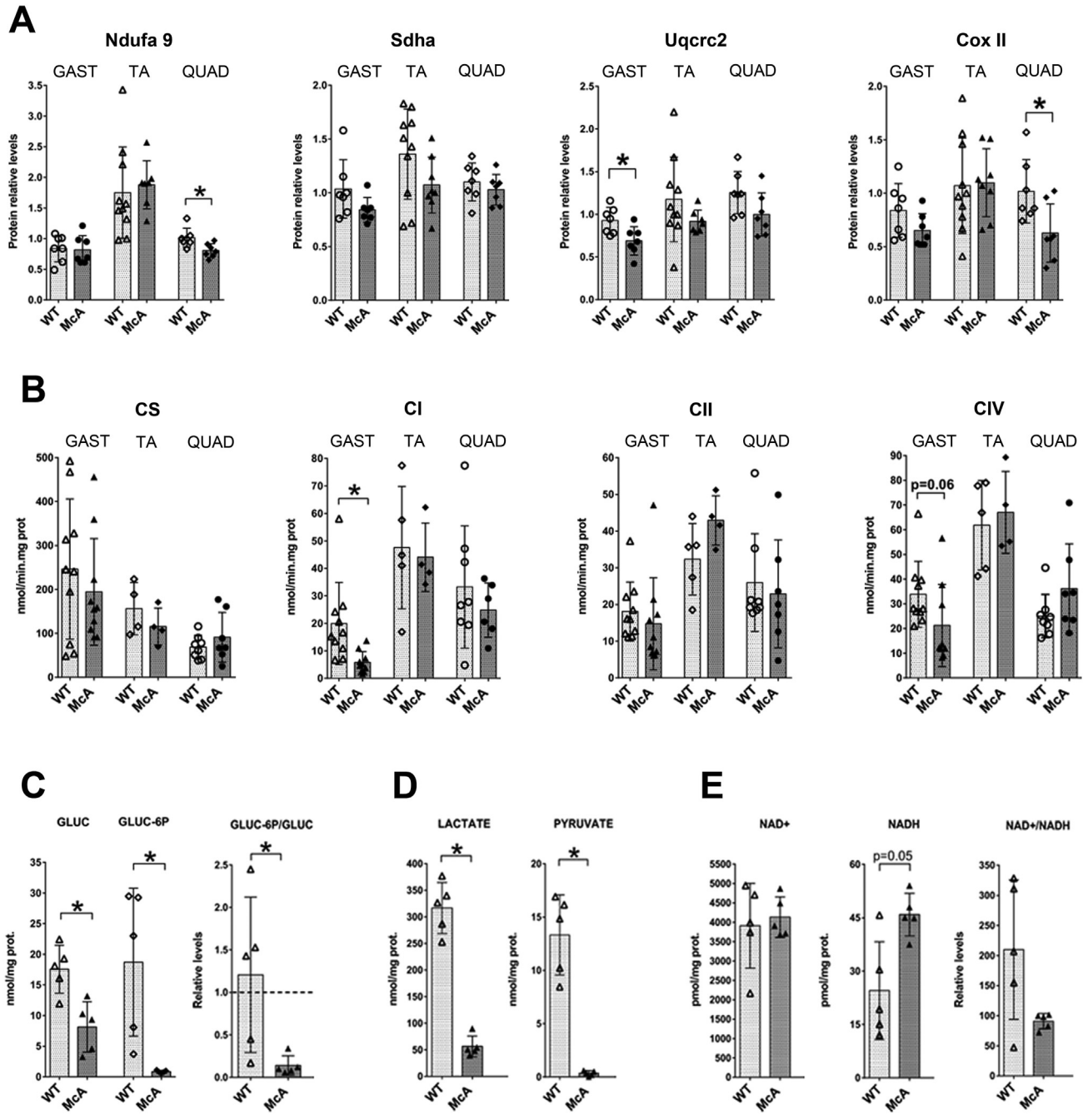

Figure 5: Analysis of OXPHOS protein levels and activity. **(A)** Western blot analysis of Ndufa9 (complex I; CI), Sdha (complex II; CII), Uqcrc2 (complex III; CIII) and CoxII (complex IV; CIV) protein relative levels in the gastrocnemius [N = 7 wild-type (57% male) and 7 McArdle mice (29% male)], tibialis anterior [N = 10 wild-type (50% male) and 8 McArdle mice (25% male)] and quadriceps (N = 7 (3 male) in both groups for the different proteins). **(B)** Citrate synthase and OXPHOS CI, CII and CIV activities in total tissue homogenates from gastrocnemius [N = 10 wild-type (60% male) and 10 McArdle mice (40% male)], tibialis anterior [N = 5 wild-type (60% male) and 4 McArdle mice (50% male)] and quadriceps [N = 8 wild-type (50% male) and 7 McArdle mice (57% male)]. **(C, D and E)** Mass spectrometry analysis of glucose, glucose-6-phosphate, lactate, pyruvate, NAD+ and NADH in total quadriceps homogenates from wild-type and McArdle mice. In these experiments, the same number of mice (N = 5) and sex distribution (40% male) was studied in the two groups. When data followed a normal distribution (Ndufa9, Sdha, Uqcrc2, and Cox II protein levels, as well as CS quadriceps activity) a Student's *t*-test was applied, whereas the non-parametric Mann–Whitney *U*-test was used when values were not normally distributed (CS activity in gastrocnemius and tibialis anterior, complex I, II and IV activities, as well as glucose, glucose-6-p, lactate, pyruvate, NAD+ and NADH levels in the quadriceps). Asterisks correspond to $p < 0.005$ in the statistic tests. **Abbreviations**: GAST: gastrocnemius; QUAD: quadriceps; TA: tibialis anterior; WT: wild-type; McA: McArdle; Ndufa9: NADH: Ubiquinone oxidoreductase subunit A9; Sdha: succinate dehydrogenase complex flavoprotein subunit A; Uqcrc2: ubiquinol-cytochrome c reductase core protein 2; Cox II: cytochrome c oxidase subunit II; CS: citrate synthase; GLUC: glucose (non-phosphorylated); GLUC-6-P: glucose-6-phosphate.

Next, we wanted to assess whether the full blockade of glycogen degradation that characterizes McArdle disease reduced glycolytic flux, further contributing to OXPHOS impairment. In this effect, mass spectrometry results indicated lower levels of glucose, glucose-6-phosphate, pyruvate and lactate but higher NADH levels in McArdle mouse muscle compared to WT (Figure 5C–E).

3.7. Peak aerobic capacity in patients

We finally aimed at providing strong corroborating evidence for a major impairment of muscle oxidative metabolism in McArdle disease patients, as reflected at the whole-body level during intense exertion through determination of the universal measure VO_{2peak}. We therefore compared the VO_{2peak} of the largest series of McArdle disease patients ever analyzed (N = 145, 34 ± 14 years) and an age and sex-matched control group (N = 133, 33 ± 13 years). The *PYGM* genotypes of patients leading to diagnosis of McArdle disease are displayed in **Supplementary File 2**. Both male (N = 82) and female (N = 63) patients showed significantly lower VO_{2peak} levels than their sex-matched controls (by −51% and −53%, respectively, Figure 6A), with only 8% of patients (both sexes combined, vs 88% of controls) reaching the minimum threshold for optimal cardiovascular health—*i.e.*, $VO_{2peak} \geq 8$ metabolic equivalents of task (MET), with 1 ME T equivalent to an oxygen uptake level of 3.5 ml O_2/kg/min.

3.8. Muscle cytoskeleton and mitochondrial network in two patients

An important step was to provide preliminary evidence whether the loss of cytoskeleton integrity with subsequent disruption of the mitochondrial network and presence of damaged mitochondria found in the skeletal muscle of McArdle mice might also occur in affected patients, thereby accounting—at least partly—for their low muscle oxidative capacity (as in turn reflected by very low VO_{2peak} values). To this end, *vastus lateralis* muscle biopsies from two patients were analyzed, with the results suggesting apparent disruption of the mitochondrial network, together with loss of intermediate filaments, actin microfilaments, and microtubules (Figure 6B). Consecutive muscle sections staining for fast MHC and SDH showed that fibers—presumably type IIA—with high mitochondrial content were the most affected ones (Figure 6B i-ii), with these preliminary data in two patients being in line with the results obtained mice. Additionally, SDH staining showed several different fibers with high amount of subsarcolemmal mitochondrial accumulation (Figure 6B iii-iv). Finally, electron microscope analysis of *vastus lateralis* biopsies in two patients showed a large amount of damaged mitochondria within subsarcolemmal and intermyofibrillar glycogen-rich regions, together with a low amount of cristae and the presence of membrane-like structures, as well as abnormally large mitochondria (Figure 6C).

4. DISCUSSION

In the present work we have analyzed whether mitochondrial network integrity and function is altered in the skeletal muscle of McArdle mouse model (with preliminary data in two patients), in order to gain insight into the potential mechanisms underpinning the poor aerobic fitness previously documented in this condition, which was corroborated here using a very large cohort. We have found that, in McArdle muscle, most damaged fibers are those with a higher mitochondrial and glycogen content (*i.e.*, type II in patients, and type IIA and IIX in mice), which show major disruption of the three main cytoskeleton components—actin microfilaments, microtubules and intermediate filaments. This, in turn, might contribute to cause a disruption of the mitochondrial network in the mouse/patient skeletal muscle fibers, together with an altered subcellular localization of mitochondrial fission and fusion proteins, as well as the SR protein calsequestrin, thereby disturbing the proper function of mitochondrial dynamics. We also found an impairment in mitochondrial content and biogenesis, a decrease in OXPHOS complex proteins and activities, together with high muscle NADH but reduced muscle levels of glucose-6-phosphate and of the glycolytic products pyruvate and lactate. In all, these results suggest that the deficiency in oxidative metabolism in McArdle disease might be caused by not only by reduced levels of OXPHOS substrates as previously reported—and corroborated here—but also by a disruption of the mitochondrial network—which was shown here in detail for the first time. The combined effect of OXPHOS deficiency and structural mitochondrial network damage and subsequent dysfunction of these organelles might help to explain why treatment with a compound with an anaplerotic role in the Krebs cycle, triheptanoin, has failed to improve muscle oxidative capacity and exercise capacity in patients with McArdle disease [35]. Indeed, although triheptanoin could replenish Krebs cycle intermediates, this positive effect might be counterbalanced by the presence of damaged mitochondria in the context of a disrupted network of these organelles, thereby suggesting that impairment in glycolytic flux is not the only mechanism underpinning the impaired aerobic capacity of these patients. In the same line, although the peak aerobic capacity of p.R50*/p.R50* mice increases significantly with regular endurance training (for eight weeks, which would be equivalent to ∼one-year duration when translated to 'human lifespan'), it still remains remarkably lower (∼by 50%) compared to untrained WT mice [9], which is in accord with findings in patients [4,36].

A major finding of the present study is that most damaged muscle fibers in McArdle mice were those with higher glycogen and mitochondrial content. In this effect, although a causative association between the amount of glycogen content, on the one hand, and the degree of mitochondrial network disruption, on the other, cannot be inferred, previous studies in McArdle mice have shown that the large muscle glycogen depots that characterize this disease cause myofibrils to tear, change direction, and split from adjacent myofibrils, while T-tubules appear misaligned to myofibrils [21]. These previous results suggest that glycogen accumulation alters the overall ultrastructure of the muscle fibers. In the present study, we have further observed that most damaged fibers presented with a remarkable disruption of intermediate and actin microfilaments and microtubules, along with a disturbance of the mitochondrial network. In this effect, it is well established that the location of mitochondria within the cell as well as the arrangement of the network formed by these organelles is highly dependent on the cytoskeleton structure [30,31,37]. In addition, the cytoskeleton, more specifically βII-tubulin, plays an important role in regulating the local diffusion of ADP through the VDAC pore in the mitochondrial outer membrane in order to control the kinetics of ATP synthesis [38,39]. Furthermore, tubulin has been recognized as an inherent mitochondrial membrane component that acts as a regulator of the mitochondrial permeability transition pore and thereby plays a role in apoptosis, supporting mitochondrial membrane potential and regulating OXPHOS [40]. Given all of the above, the large glycogen deposits inside the skeletal muscle fibers of mice and patients are likely to alter the overall structure of these cells (including the different cytoskeleton components) and subsequently the localization and network arrangement of mitochondria within the cell, thereby potentially affecting, at least partly, the function of these organelles. Additionally, and probably as a consequence of mitochondrial network disruption, we also observed an altered subcellular localization of the

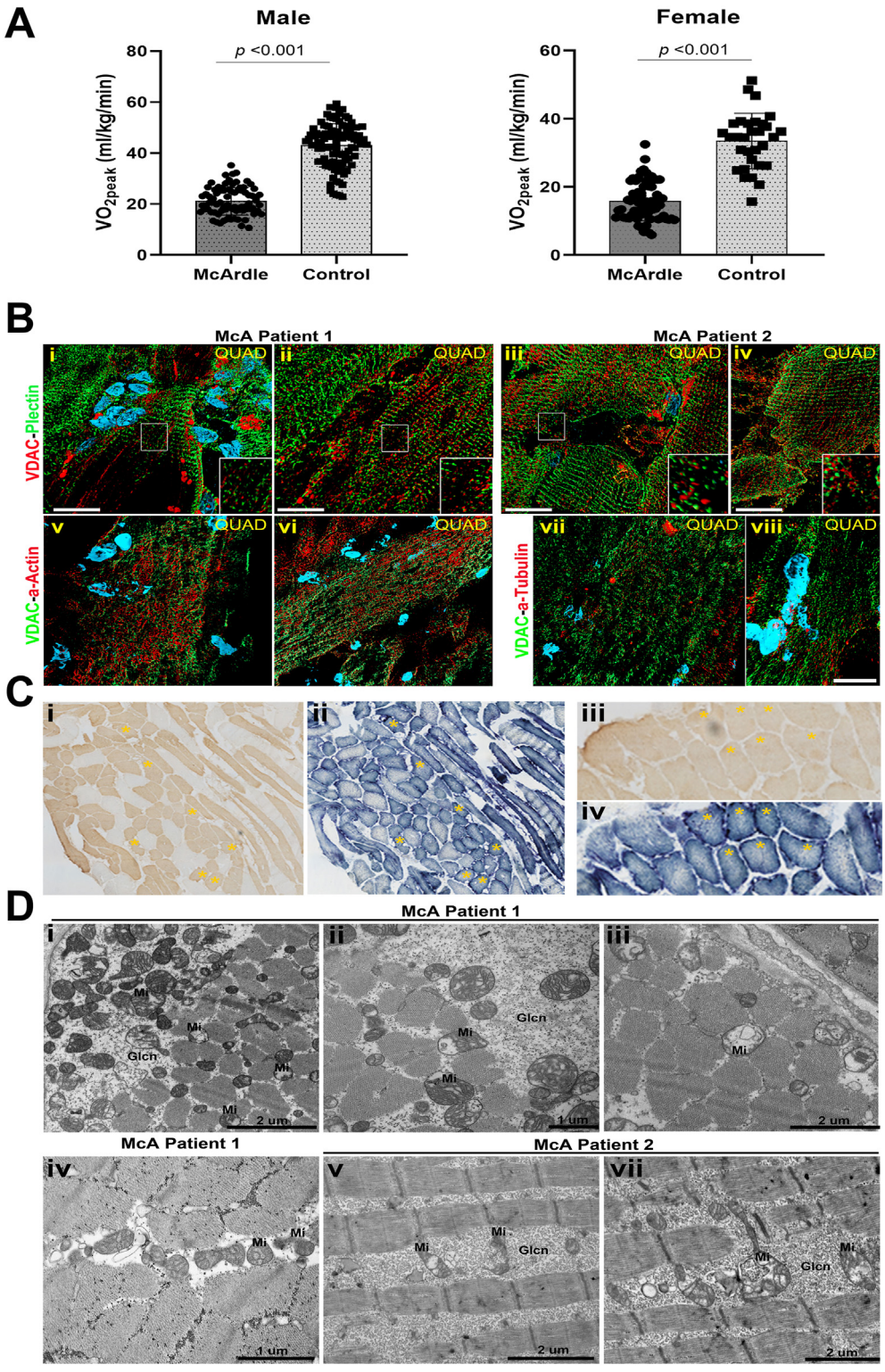

Figure 6: Peak oxygen uptake (VO2peak) and analysis of the cytoskeleton and mitochondrial network integrity in patients with McArdle disease. (A) VO2peak levels of patients with McArdle disease (N = 145) versus control individuals (N = 133). (B) Immunofluorescence analysis of the cytoskeleton and mitochondrial network integrity in quadriceps biopsies from two different McArdle disease patients; VDAC (red) and plectin (green) immunofluorescence staining (i-iv); VDAC (green) and α-actin (red) immunofluorescence staining (v-viii); cell nucleus (blue) are stained with DAPI. Scale bars correspond to 25 μm. (C) Consecutive quadriceps sections staining for fast muscle fibers and SDH activity; i and iii) fast muscle fibers immunohistochemical staining; ii and iv) SDH activity staining; yellow asterisks mark identical muscle fibers in i) and ii), as well as in iii) and iv). (D) Electronic microscopy analysis of mitochondria ultrastructure in quadriceps biopsies from two different McArdle disease patients. Scale bars correspond to 1 or 2 μm as indicated. Abbreviations; QUAD: quadriceps; McA: McArdle; Glcn: glycogen and Mi: mitochondria.

different proteins involved in mitochondrial fission (Drp1 and Fis 1) and fusion (Mfn2 and Opa1), as well as lower levels of Mfn2 in the skeletal muscle of McArdle mice, possibly leading to lower mitochondrial fusion. Furthermore, Drp1 frequently co-localized with isolated (and enlarged) mitochondria, thereby suggesting that mitochondrial fission was actively involved in the separation of potentially damaged mitochondria from the network. Besides their negative effect on mitochondrial dynamics, changes in the cellular distribution of the different fission/fusion proteins might also affect mitochondrial integrity, membrane potential and oxidative metabolism. In this regard, it has been observed that Opa1 is involved in maintaining the shape of mitochondrial cristae by stabilizing respiratory chain super-complexes [41–43], while loss of Mfn2 function causes metabolic alterations in mitochondria (i.e., lower membrane potential and cellular oxygen consumption, as well as depressed substrate oxidation) with the absence of both mitofusins Opa1 and Mfn2 leading to severe mtDNA depletion [33]. Consistent with this, we observed an impaired mitochondrial content and biogenesis as well as a decrease in OXPHOS complex proteins and activities in the skeletal muscle of McArdle mice. Additionally, we report the presence of c-shaped or "donut" like mitochondria, a phenomenon that has been previously associated with oxidative stress and/or impaired energy production [29,44]; in this regard, the observed increased levels of the Nrf2 protein in the skeletal muscle of McArdle mice might represent a compensatory adaptation aiming at reducing the oxidative stress caused by mitochondrial metabolism impairment

Mitochondrial network disruption might also affect the interaction of mitochondria with other organelles such as SR, lysosomes or lipid droplets. In this regard, mitochondrial fission 1 protein (commonly abbreviated as 'FIS1'), which is known to be involved in mitochondria/SR interaction [45], showed an abnormal subcellular localization in the skeletal muscle of McAdle mice. This, together with the fact that mitochondria/SR contact sites might be disrupted, would suggest that mitochondrial calcium metabolism and lipid homeostasis could also be affected.

Concerning the aerobic capacity of the largest series of patients with McArdle disease ever evaluated with exercise testing, we showed that the VO_{2peak} level of these individuals was much lower compared to healthy controls, which is in line with previous findings indicating impaired oxidative metabolism and/or low VO_{2peak} (which is also an indicator of peak muscle oxidative capacity) in patients with this condition [7,13,14,27,46–51]. Additionally, muscle biopsy analyses from two patients suggested similar figures to those found in mice—loss of mitochondrial and cytoskeleton integrity and disruption of the mitochondrial network, especially in type II (glycogen-reliant) fibers—thereby providing preliminary support to the notion that mitochondrial network disruption underpins, at least partly, the impairment in muscle oxidative capacity that characterizes this disease. More research in larger patient cohorts is needed to corroborate our pilot results in only two individuals.

On the other hand, the role of mitochondria in the pathophysiology of GSDs other than McArdle disease has not been extensively studied. In GSD Ia (deficiency of the catalytic activity of glucose-6-phosphatase, with subsequent intracellular accumulation of glycogen in liver, kidney and small intestines), a decreased mitochondrial content and membrane potential, deranged mitochondria ultrastructure, impaired oxidative phosphorylation and changes in Krebs cycle metabolites have been described in cell cultures as well as in the mouse model for this condition [52], with some authors also reporting a decrease in mitochondrial number [53] or the presence of swollen and deformed mitochondria [54]. In the case of GSD II (Pompe disease), multiple mitochondrial defects have been described in mouse models and patients, including a profound dysregulation of calcium homeostasis, mitochondrial calcium overload, increase in reactive oxygen species and caspase-independent apoptosis, and decrease in mitochondrial membrane potential as well as in the ATP production capacity of mitochondria [55]. Loss of function variants in the chromosome 2 open reading frame 69 (*C2orf69*) gene, which controls the levels of the glycogen branching enzyme, affects mitochondrial membrane potential and oxidative respiration in cultured neurons, consistent with a glycogen storage-associated mitochondriopathy [56]. Similarly, altered mitochondrial bioenergetics has been reported in the liver of heterozygous *Gbe1*$^{+/-}$ mice [57]. Further studies are needed to corroborate the implication of muscle mitochondrial impairment in the pathophysiology of other GSDs—especially those, like McArdle disease, associated with exercise intolerance and low aerobic capacity. On the other hand, the present findings should be kept in mind when assessing therapeutic approaches for McArdle disease and other GSDs affecting the skeletal muscle. Indeed, full restoration of muscle oxidative capacity might not be always possible with drug or exercise intervention in the context of severe mitochondrial network disruption inside this tissue.

5. CONCLUSIONS

A hallmark of McArdle disease, severe impairment in muscle oxidative capacity as reflected by very low VO_{2peak} values in affected individuals, could be explained not only by a reduced glycolytic flux due to the inherited metabolic blockade in muscle glycogen breakdown, but also possibly by a disruption of the mitochondrial network in skeletal muscle fibers due to abnormally large glycogen depots, at least in those fibers with a higher capacity for accumulating this substrate. Pending corroboration studies in more patients with McArdle disease, the present findings might pave the way for future research addressing the potential involvement of mitochondrial network alterations in the pathophysiology of other GSDs.

ETHICS APPROVAL

All experimental procedures were approved by the Vall d'Hebron Institutional Review Board (protocol number 58/17 CEEA; 35/04/08) and were conducted in accordance with the European Convention for the Protection of Vertebrate Animals used for Experimental and Other Scientific Purposes (ETS1 2 3) and Spanish laws (32/2007 and R.D. 1201/2005). The study in humans adhered the ethics guidelines of the Declaration of Helsinki, and was approved by the Ethics Committee of Hospital 12 de Octubre, Madrid, Spain (approval number 16/081). All participants were informed about the study procedures and signed a written informed consent.

CONSENT FOR PUBLICATION

Not applicable.

AVAILABILITY OF DATA AND MATERIAL

The datasets generated during and/or analysed during the current study are available from the corresponding author on reasonable request.

FUNDING

The present study was funded by grants received from the Fondo de Investigaciones Sanitarias (FIS, PI17/02052, PI18/00139, PI19/01313,

and PI20/00645) and cofunded by 'Fondos FEDER'. Gisela Nogales-Gadea and Carmen Fiuza-Luces are supported by the Miguel Servet research contracts (ISCIII CD14/00032 and CP18/00034, respectively and cofounded by Fondos FEDER'). Research by Pedro L. Valenzuela is funded by a postdoctoral contract granted by Instituto de Salud Carlos III (Sara Borrell, CD21/00138). Monica Villarreal Salazar is supported by the Mexican National Council for Science and Technology (CONACYT).

AUTHORS CONTRIBUTIONS

MVS, ARM performed all the mice experiments, AS, AL, and CFL performed patients' tests, JCRA performed mass spectrometry analyses, GNG, ALA, MAM, JA, JV and AL made major contributions in the writing and revision of the manuscript, while TOK and TP designed the experiments and TP wrote the first manuscript draft.

DATA AVAILABILITY

Data will be made available on request.

ACKNOWLEDGEMENTS

Authors would like to thank Javier Torres Torronteras, Yolanda Cámara and Ramon Martí Seves for their constant scientific inputs.

CONFLICT OF INTERESTS

The author(s) declare no conflict of interest.

APPENDIX A. SUPPLEMENTARY DATA

Supplementary data to this article can be found online at https://doi.org/10.1016/j.molmet.2022.101648.

REFERENCES

[1] Nogales-Gadea G, Pinos T, Andreu AL, Martin MA, Arenas J, Lucia A. Next-generation sequencing to estimate the prevalence of a great unknown: McArdle disease. Genet Med 2015;17(8):679–80.

[2] De Castro M, Johnston J, Biesecker L. Determining the prevalence of McArdle disease from gene frequency by analysis of next-generation sequencing data. Genet Med 2015;17(12):1002–6.

[3] Munguia-Izquierdo D, Santalla A, Lucia A. Cardiorespiratory fitness, physical activity, and quality of life in patients with McArdle disease. Med Sci Sports Exerc 2015;47(4):799–808.

[4] Mate-Munoz JL, Moran M, Perez M, Chamorro-Vina C, Gomez-Gallego F, Santiago C, et al. Favorable responses to acute and chronic exercise in McArdle patients. Clin J Sport Med 2007;17(4):297–303.

[5] Ozemek C, Laddu DR, Lavie CJ, Claeys H, Kaminsky LA, Ross R, et al. An update on the role of cardiorespiratory fitness, structured exercise and lifestyle physical activity in preventing cardiovascular disease and health risk. Prog Cardiovasc Dis 2018;61(5–6):484–90.

[6] Ross R, Blair SN, Arena R, Church TS, Despres JP, Franklin BA, et al. Importance of assessing cardiorespiratory fitness in clinical practice: a case for fitness as a clinical vital sign: a scientific statement from the American Heart association. Circulation 2016;134(24):e653–99.

[7] Scalco RS, Lucia A, Santalla A, Martinuzzi A, Vavla M, Reni G, et al. Data from the European registry for patients with McArdle disease and other muscle glycogenoses (EUROMAC). Orphanet J Rare Dis 2020;15(1):330.

[8] Villarreal-Salazar M, Brull A, Nogales-Gadea G, Andreu AL, Martin MA, Arenas J, et al. Preclinical research in McArdle disease: a Review of research models and therapeutic strategies. Genes 2021;13(1).

[9] Fiuza-Luces C, Santos-Lozano A, Llavero F, Campo R, Nogales-Gadea G, Diez-Bermejo J, et al. Muscle molecular adaptations to endurance exercise training are conditioned by glycogen availability: a proteomics-based analysis in the McArdle mouse model. J Physiol 2018;596(6):1035–61.

[10] Grassi B, Porcelli S, Marzorati M, Lanfranconi F, Vago P, Marconi C, et al. Metabolic myopathies: functional evaluation by analysis of oxygen uptake kinetics. Med Sci Sports Exerc 2009;41(12):2120–7.

[11] Siciliano G, Rossi B, Martini A, Angelini C, Martinuzzi A, Lodi R, et al. Myophosphorylase deficiency affects muscle mitochondrial respiration as shown by 31P-MR spectroscopy in a case with associated multifocal encephalopathy. J Neurol Sci 1995;128(1):84–91.

[12] Lucia A, Nogales-Gadea G, Perez M, Martin MA, Andreu AL, Arenas J. McArdle disease: what do neurologists need to know? Nat Clin Pract Neurol 2008;4(10):568–77.

[13] Haller RG, Lewis SF, Cook JD, Blomqvist CG. Myophosphorylase deficiency impairs muscle oxidative metabolism. Ann Neurol 1985;17(2):196–9.

[14] De Stefano N, Argov Z, Matthews PM, Karpati G, Arnold DL. Impairment of muscle mitochondrial oxidative metabolism in McArdles's disease. Muscle Nerve 1996;19(6):764–9.

[15] Fiuza-Luces C, Nogales-Gadea G, Garcia-Consuegra I, Pareja-Galeano H, Rufian-Vazquez L, Perez LM, et al. Muscle signaling in exercise intolerance: insights from the McArdle mouse model. Med Sci Sports Exerc 2016;48(8):1448–58.

[16] Dong F, Zhu M, Zheng F, Fu C. Mitochondrial fusion and fission are required for proper mitochondrial function and cell proliferation in fission yeast. FEBS J 2022;289(1):262–78.

[17] Gonzalez-Freire M, Scalzo P, D'Agostino J, Moore ZA, Diaz-Ruiz A, Fabbri E, et al. Skeletal muscle ex vivo mitochondrial respiration parallels decline in vivo oxidative capacity, cardiorespiratory fitness, and muscle strength: the Baltimore Longitudinal Study of Aging. Aging Cell 2018;17(2).

[18] Weibel ER, Hoppeler H. Exercise-induced maximal metabolic rate scales with muscle aerobic capacity. J Exp Biol 2005;208(Pt 9):1635–44.

[19] Nogales-Gadea G, Pinos T, Lucia A, Arenas J, Camara Y, Brull A, et al. Knock-in mice for the R50X mutation in the PYGM gene present with McArdle disease. Brain 2012;135(Pt 7):2048–57.

[20] Real-Martinez A, Brull A, Huerta J, Tarrasó G, Lucia A, Martin M, et al. Low survival rate and muscle fiber-dependent aging effects in the McArdle disease mouse model. Sci Rep 2019;9(1):5116.

[21] Krag TO, Pinos T, Nielsen TL, Brull A, Andreu AL, Vissing J. Differential muscle involvement in mice and humans affected by McArdle disease. J Neuropathol Exp Neurol 2016;75(5):441–54.

[22] Brull A, de Luna N, Blanco-Grau A, Lucia A, Martin MA, Arenas J, et al. Phenotype consequences of myophosphorylase dysfunction: insights from the McArdle mouse model. J Physiol 2015;593(12):2693–706.

[23] Dubowitz C, Sewry CA, Oldfors A. Muscle biopsy a practical approach. 5th ed 2020.

[24] Andreu AL, Martinez R, Marti R, Garcia-Arumi E. Quantification of mitochondrial DNA copy number: pre-analytical factors. Mitochondrion 2009;9(4):242–6.

[25] Nogales-Gadea G, Rubio JC, Fernandez-Cadenas I, Garcia-Consuegra I, Lucia A, Cabello A, et al. Expression of the muscle glycogen phosphorylase gene in patients with McArdle disease: the role of nonsense-mediated mRNA decay. Hum Mutat 2008;29(2):277–83.

[26] Medja F, Allouche S, Frachon P, Jardel C, Malgat M, Mousson de Camaret B, et al. Development and implementation of standardized respiratory chain spectrophotometric assays for clinical diagnosis. Mitochondrion 2009;9(5):331–9.

[27] Santalla A, Nogales-Gadea G, Encinar AB, Vieitez I, Gonzalez-Quintana A, Serrano-Lorenzo P, et al. Genotypic and phenotypic features of all Spanish

patients with McArdle disease: a 2016 update. BMC Genom 2017;18(Suppl 8):819.
[28] Glancy B, Kim Y, Katti P, Willingham TB. The functional impact of mitochondrial structure across subcellular scales. Front Physiol 2020;11:541040.
[29] Ding WX, Li M, Biazik JM, Morgan DG, Guo F, Ni HM, et al. Electron microscopic analysis of a spherical mitochondrial structure. J Biol Chem 2012;287(50):42373–8.
[30] Mado K, Chekulayev V, Shevchuk I, Puurand M, Tepp K, Kaambre T. On the role of tubulin, plectin, desmin, and vimentin in the regulation of mitochondrial energy fluxes in muscle cells. Am J Physiol Cell Physiol 2019;316(5):C657–67.
[31] Moore AS, Holzbaur ELF. Mitochondrial-cytoskeletal interactions: dynamic associations that facilitate network function and remodeling. Curr Opin Physiol 2018;3:94–100.
[32] Chen H, Chan DC. Mitochondrial dynamics–fusion, fission, movement, and mitophagy–in neurodegenerative diseases. Hum Mol Genet 2009;18(R2):R169–76.
[33] Chen H, Vermulst M, Wang YE, Chomyn A, Prolla TA, McCaffery JM, et al. Mitochondrial fusion is required for mtDNA stability in skeletal muscle and tolerance of mtDNA mutations. Cell 2010;141(2):280–9.
[34] Holmstrom KM, Kostov RV, Dinkova-Kostova AT. The multifaceted role of Nrf2 in mitochondrial function. Curr Opin Toxicol 2016;1:80–91.
[35] Madsen KL, Laforet P, Buch AE, Stemmerik MG, Ottolenghi C, Hatem SN, et al. No effect of triheptanoin on exercise performance in McArdle disease. Ann Clin Transl Neurol 2019;6(10):1949–60.
[36] Santalla A, Valenzuela PL, Rodriguez-Lopez C, Rodriguez-Gomez I, Nogales-Gadea G, Pinos T, et al. Long-term exercise intervention in patients with McArdle disease: clinical and aerobic fitness benefits. Med Sci Sports Exerc 2022;54(8):1231–41.
[37] Varikmaa M, Bagur R, Kaambre T, Grichine A, Timohhina N, Tepp K, et al. Role of mitochondria-cytoskeleton interactions in respiration regulation and mitochondrial organization in striated muscles. Biochim Biophys Acta 2014;1837(2):232–45.
[38] Tepp K, Mado K, Varikmaa M, Klepinin A, Timohhina N, Shevchuk I, et al. The role of tubulin in the mitochondrial metabolism and arrangement in muscle cells. J Bioenerg Biomembr 2014;46(5):421–34.
[39] Kuznetsov AV, Javadov S, Guzun R, Grimm M, Saks V. Cytoskeleton and regulation of mitochondrial function: the role of beta-tubulin II. Front Physiol 2013;4:82.
[40] Carre M, Andre N, Carles G, Borghi H, Brichese L, Briand C, et al. Tubulin is an inherent component of mitochondrial membranes that interacts with the voltage-dependent anion channel. J Biol Chem 2002;277(37):33664–9.
[41] Quintana-Cabrera R, Quirin C, Glytsou C, Corrado M, Urbani A, Pellattiero A, et al. The cristae modulator Optic atrophy 1 requires mitochondrial ATP synthase oligomers to safeguard mitochondrial function. Nat Commun 2018;9(1):3399.
[42] Frezza C, Cipolat S, Martins de Brito O, Micaroni M, Beznoussenko GV, Rudka T, et al. OPA1 controls apoptotic cristae remodeling independently from mitochondrial fusion. Cell 2006;126(1):177–89.
[43] Lee H, Smith SB, Yoon Y. The short variant of the mitochondrial dynamin OPA1 maintains mitochondrial energetics and cristae structure. J Biol Chem 2017;292(17):7115–30.
[44] Stahon KE, Bastian C, Griffith S, Kidd GJ, Brunet S, Baltan S. Age-related changes in axonal and mitochondrial ultrastructure and function in white matter. J Neurosci 2016;36(39):9990–10001.
[45] Iwasawa R, Mahul-Mellier AL, Datler C, Pazarentzos E, Grimm S. Fis1 and Bap31 bridge the mitochondria-ER interface to establish a platform for apoptosis induction. EMBO J 2011;30(3):556–68.
[46] Pizzamiglio C, Mahroo OA, Khan KN, Patasin M, Quinlivan R. Phenotype and genotype of 197 British patients with McArdle disease: an observational single-centre study. J Inherit Metab Dis 2021;44(6):1409–18.
[47] Lewis SF, Haller RG. 1986. The pathophysiology of McArdle's disease: clues to regulation in exercise and fatigue. J Appl Physiol 1985;61(2):391–401.
[48] Hagberg JM, Coyle EF, Carroll JE, Miller JM, Martin WH, Brooke MH. Exercise hyperventilation in patients with McArdle's disease. J Appl Physiol Respir Environ Exerc Physiol 1982;52(4):991–4.
[49] Carroll JE, Hagberg JM, Brooke MH, Shumate JB. Bicycle ergometry and gas exchange measurements in neuromuscular diseases. Arch Neurol 1979;36(8):457–61.
[50] Bank W, Chance B. An oxidative defect in metabolic myopathies: diagnosis by noninvasive tissue oximetry. Ann Neurol 1994;36(6):830–7.
[51] Andersen KL, Lund-Johansen P, Clausen G. Metabolic and circulatory responses to muscular exercise in a subject with glycogen storage disease (McArdle's Disease). Scand J Clin Lab Invest 1969;24(2):105–13.
[52] Farah BL, Sinha RA, Wu Y, Singh BK, Lim A, Hirayama M, et al. Hepatic mitochondrial dysfunction is a feature of glycogen storage disease type Ia (GSDIa). Sci Rep 2017;7:44408.
[53] Riede UN, Spycher MA, Gitzelmann R. Glycogenosis type I (glucose 6-phosphatase deficiency): I. Ultrastructural morphometric analysis of juvenile liver cells. Pathol Res Pract 1980;167(1):136–50.
[54] Cho JH, Kim GY, Pan CJ, Anduaga J, Choi EJ, Mansfield BC, et al. Down-regulation of SIRT1 signaling underlies hepatic autophagy impairment in glycogen storage disease type Ia. PLoS Genet 2017;13(5):e1006819.
[55] Lim JA, Li L, Kakhlon O, Myerowitz R, Raben N. Defects in calcium homeostasis and mitochondria can be reversed in Pompe disease. Autophagy 2015;11(2):385–402.
[56] Wong HH, Seet SH, Maier M, Gurel A, Traspas RM, Lee C, et al. Loss of C2orf69 defines a fatal autoinflammatory syndrome in humans and zebrafish that evokes a glycogen-storage-associated mitochondriopathy. Am J Hum Genet 2021;108(7):1301–17.
[57] Malinska D, Testoni G, Bejtka M, Duran J, Guinovart JJ, Duszynski J. Alteration of mitochondrial function in the livers of mice with glycogen branching enzyme deficiency. Biochimie 2021;186:28–32.

